Blind Image Deblurring Using Gradient Prior and Sparse Prior

Su Xiao

***Abstract*—To precisely estimate blur kernels (BKs) and obtain high-quality latent images (LIs), we present an efficient blind image deblurring (BID) algorithm via a gradient prior and an enhanced sparse prior. The proposed algorithm decomposes BID into two phases: multiscale blur estimation (MSBE) and image deconvolution (ID). The former focuses on precise BKs, whereas the latter focuses on high-quality LIs. In the MSBE phase, significant image gradients and an enhanced sparse prior are used to estimate BKs. To this end, we build an MSBE model using a hyper-Laplacian gradient (HLG) prior and sparsity-inducing $l_{2,1}$-regularization. $l_{2,1}$-regularization imposes enhanced sparsity on the BKs to be estimated, and the HLG prior characterizes the true distribution of image gradients. We use a method derived from half-quadratic splitting (HQS) to handle the built MSBE model by decoupling it into simpler subproblems. Subsequently, these subproblems are solved by efficient and concise methods. In the MSBE phase, we also adopt a multiscale process to avoid local optima of the estimated BKs and adaptively update a penalty parameter to accelerate the iteration. In the ID phase, SotA restoration algorithms are employed by the proposed BID algorithm to obtain competitive final LIs. The experiments are conducted on several baseline datasets to evaluate our BID algorithm. Under the evaluation criteria of success-rate (SR), SSDE, PSNR, SSIM, vision effect, and running time (RT), our study shows apparent advantages compared with some SotA BID algorithms. These advantages include but are not limited to reducing the RT; obtaining higher PSNRs, SSIMs, and SRs; decreasing SSDEs; and obtaining high-quality LIs without artifacts.**

***Index Terms*—BID, blur estimation, image deconvolution, sparse priors, gradient priors, HQS.**

I. Introduction

In daily life, exciting scenes and moments are often encountered, and the failure to capture clear images of these scenes is undoubtedly regrettable. With the popularization of digital imaging devices, opportunities to experience this regret have increased. To compensate for this, researchers have taken several remedial measures, among which BID is the most effective and economical. BID aims to estimate BKs and obtain LIs from given degraded images and selected priors. For an extended period, the consensus of researchers in this field has been that the true and effective statistical characteristics of images and blur are the foundation for solving BID problems. Therefore, in the following review of related works, we mainly focus on the priors of BKs and LIs used by SotA BID algorithms.

Because the priors of LIs and BKs are statistical concepts, BID algorithms were first proposed based on the MAP or Bayesian frameworks. Fergus et al. [1] reported that image gradients follow heavy-tailed distributions and that BKs are sparse; therefore, they used a Gaussian mixture model and a sparse prior to characterize them. Dong et al. [2] applied a hyper-Laplacian prior and l_1-regularization to LIs and BKs, respectively. To eliminate outliers, they presented a new data-fidelity to replace the l_2-norm-based one. Under the MAP framework, Javaran et al. [3] used first-order and second-order gradient priors to estimate LIs and a l_1-regularization model to estimate sparse BKs. To avoid MRF defects, Liu et al. [4] developed an SGF prior for characterizing the statistical distribution of images.

Due to the drawbacks of the MAP and Bayesian frameworks, optimization-based algorithms have become dominant candidates in this field. Pan et al. [5] presented a BID algorithm using an HL prior of LIs and l_1-sparsity of BKs to eliminate outliers. Yan et al. [6] presented an EC prior derived from BC and DC priors and used it with a gradient prior for BID. Zhang et al. [7] utilized a gradient prior and a sparse prior on BKs to achieve good sparseness and remove noise. When modeling the BID problem, Jin et al. [8] employed the l_p-norm to normalize sparse BKs and adopted a gradient prior for LIs. To accurately estimate Bks, Bai et al. [9] first constructed skeleton images with bimodal distributions and subsequently designed a gradient prior based on the graph for these images. Yang et al. [10] presented a new BID algorithm based on edge selection by embedding a gradient prior into a VEM method. Because the maximum gradient of an image patch decreases after being blurred, Chen et al. [11] presented an LMG prior for LIs to boost BID. In the frequency domain, Anwar et al. [12] presented a CS prior that regards LIs as sparse bandpass components of similar clear images. Liu et al. [13] imposed an SA prior and a Gaussian prior on LIs and BKs to reduce artifacts. Sheng et al. [14] associated BID with depth images represented by the MRF prior and estimated LIs by alternating between deblurring and depth filling. In the spatial domain, Pan et al. [15] constructed a phase-only image prior for directly estimating spatially sparse BKs. Peng et al. [16] used a sparse prior of features to restore clear images and BKs to eliminate the influence of image blur. When handling minimization problems, these optimization-based BID algorithms primarily adopt methods such as PALM [17], HQS [18], and ADMM [19].

Recently, BID algorithms that use various deep neural networks (DNNs) have attracted much attention. DNNs were initially used to estimate BKs [20] and subsequently used for image-to-image restoration [21]. Because clear images and BKs generally do not exist, DNN-based BID algorithms are heavily dependent on training datasets. This dependency may introduce uncertainty to BID (as satisfactory results are not guaranteed) and restrict the generality of these BID algorithms. For example, Fig. 1 shows a DNN-based BID algorithm that fails to process degraded images from the

Manuscript received September 12, 2023; revised April 4, 2024. This work is supported by the Natural Science Research Project of Anhui Provincial Department of Education (Grant No. 2022AH050370).

Su Xiao is a professor of School of Computer Science and Technology, Huaibei Normal University, Huaibei 235000, Anhui, China (e-mail: csxiaosu@139.com).

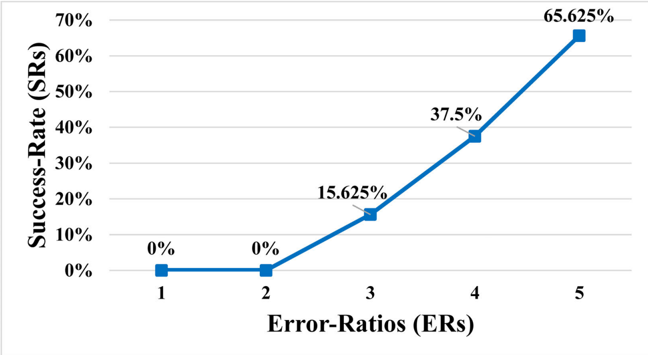

Fig. 1: Results of Processing the Levin Dataset Using a DNN-based BID Algorithm

Levin dataset [22].

Currently, typical issues in BID include but are not limited to the following: the priors adopted are not consistent with the true gradient distribution of LIs; the noise and adverse details are not effectively handled, resulting in the failure of image priors; and the priors sometimes fail to promote blur sparsity and cause computing difficulties. To address these existing issues, we focus on optimization-based BID and propose a novel and efficient algorithm. The proposed algorithm divides BID into MSBE and ID phases. In the MSBE phase, an HLG prior and a sparse prior are used to characterize LIs and BKs, respectively. BKs are robustly estimated by effective methods and strategies. In the ID phase, the estimated BKs and SotA ID algorithms are employed to obtain the final high-quality LIs. The remaining sections are described as below. Section II overviews the skeleton of our work and summarizes its contributions. Section III builds an MSBE model and presents its solution. Section IV discusses methods for obtaining final LIs. Section V presents comprehensive BID experiments on different benchmark datasets. The final section provides a summary and outlook for this study.

II. Framework of Our Study

The skeleton of our study is illustrated in Fig. 2. Because intermediate LIs are prone to detail loss, the proposed algorithm divides BID into two phases, MSBE and ID, to mitigate unpleasant restoration results. In the MSBE phase, sparse BKs are robustly estimated by a multiscale process [1]. Specifically, image pyramids are first constructed for blur estimation, and BKs are subsequently estimated layer-by-layer, moving from the coarsest one to the finest one, until full-size BKs are generated. In the ID phase, estimated BKs are used to obtain the final LIs. Levin et al. [2] noted that two-phase BID is more effective than estimating BKs and restoring LIs simultaneously.

The contributions of our BID algorithm are summarized below.

- We use a precise HLG prior to characterize the LIs and use a sparse $l_{2,1}$-regularization to enhance and promote the sparsity of BKs, generating high-quality BID results.
- The built MSBE model is decoupled into simpler subproblems by a method derived from HQS, and the generated subproblems are efficiently solved using fast Fourier transforms (FFTs), the GST_q algorithm [23], and soft-thresholding [24].
- To enhance the robustness of the MSBE phase, we apply a l_0-smoothing algorithm [25] to the gradients of intermediate LIs to remove adverse details and sharpen salient edges. We then use refined gradients to estimate BKs.
- Iterations are accelerated by automatic parameter updates, and a multiscale process is used to avoid local optimal solutions.
- Robust MSBE results and SotA ID algorithms ensure high-quality LIs.

III. MSBE Phase

Supposing that D, b, L, and n are degraded images, BKs, LIs, and noise, respectively, image degradation is expressed as

$$D = b \otimes L + n, \tag{1}$$

where $\otimes$ represents the convolution operation. In practical applications, D is known, while b and L are unknown. We cannot obtain ideal BKs or LIs by directly solving (1), because it is ill-posed. A well-posed BID is expressed as a minimization problem

$$(L^{k+1}, b^{k+1}) = \arg\min_{L,b} \frac{1}{2}\|b \otimes L - D\|_2^2 + \Phi_1(L) + \Phi_2(b), \tag{2}$$

where $\frac{1}{2}\|b \otimes L\text{-}D\|_2^2$ ensures that the LIs are consistent with the corresponding degraded images, and Φ_1 and Φ_2 are regularizers that enforce priors on LIs and BKs, respectively. For a vector z=$[z_1, z_2, ..., z_m]^T$, its l_p-norm is $\|z\|_p$=$(\sum_i |z_i|^p)^{\frac{1}{p}}$. At present, existing SotA BID algorithms adopt statistical priors, as well as effective optimization schemes, for natural images and BKs. Therefore, in the following sections, we elaborate on these key research topics.

A. Built MSBE model

The statistical analysis revealed that the gradient distribution of the images was heavy-tailed [26]. Although some novel image priors have been newly presented in recent years, simple heavy-tailed priors still demonstrate competitive advantages in artifact removal and computational efficiency. To precisely model the gradient distribution of LIs, we impose an HLG prior [27] on the distribution to yield

$$(L^{k+1}, b^{k+1}) = \arg\min_{L,b} \frac{1}{2}\|b \otimes L - D\|_2^2 + \alpha\|\nabla L\|_{\frac{2}{3}} + \Phi_2(b), \tag{3}$$

where ∇ is the gradient operator generated by the filters ∇_1=[1,-1] and ∇_2=$[1,\text{-}1]^T$; ∇L=$[\nabla_1 L,\ \nabla_2 L]^T$ is the gradient image of L; and α>0 is a constant that adjusts the regularization on LIs.

The sparsity of BKs is a simple but dominant prior that is almost the only reliable and effective prior for complex MSBE problems in various situations. The sparsity of BKs can also be exemplified by statistical results on some benchmark datasets. For example, as shown in Fig. 3, the statistical results of 2700 BKs from the Sun dataset [28] support the sparsity of BKs.

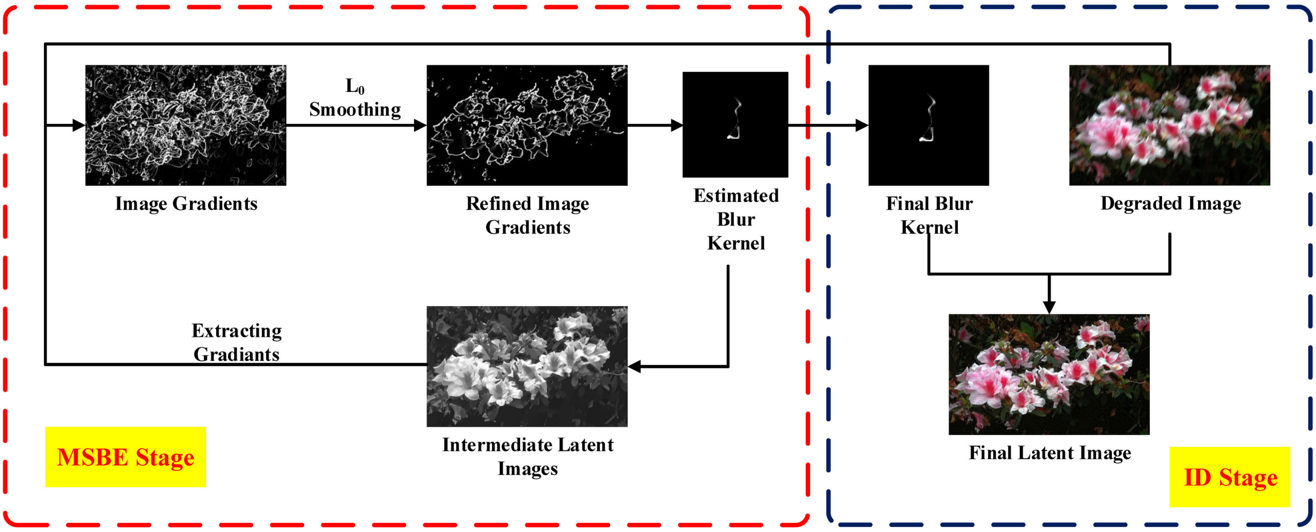

Fig. 2: Skeleton of Our Study

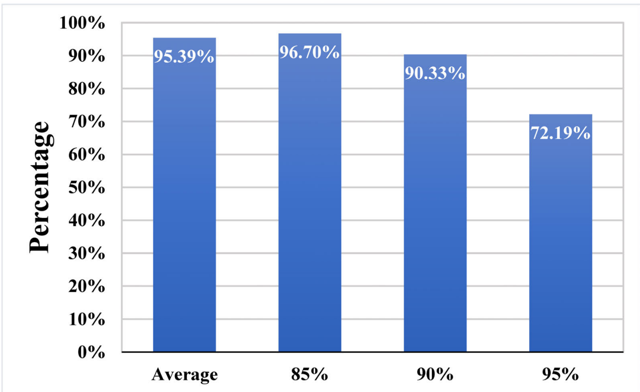

Fig. 3: Statistics on the BKs from the Sun Dataset. 85% indicates that the BKs with zero elements no less than 85%, and 90% and 95% are similar.

To induce the sparsity of BKs, most optimization-based BID algorithms employ the quadratic l_2-norm, l_1-norm, and l_0-norm as regularizers. l_2-regularization assumes that BKs satisfy the Gaussian distribution; however, this assumption is not statistically supported and tends to generate dense kernels. l_0-regularization results in an NP-hard problem and generates unnatural LIs. To robustly estimate BKs, we use the $l_{2,1}$-norm as the regularizer. As an enhanced l_1-regularization, $l_{2,1}$-regularization not only results in sparser solutions but also promotes group sparsity to effectively suppress noise in BKs.

Our MSBE model is ultimately formulated as

$$(L^{k+1}, b^{k+1}) = \arg\min_{L,b} \frac{1}{2}\|b \otimes L - D\|_2^2 + \alpha\|\nabla L\|_{\frac{2}{3}} + \beta\|b\|_{2,1}, \tag{4}$$

where $\beta>0$ is a constant that adjusts the regularization on BKs. For a matrix $A= [a_1^T, a_2^T, \dots, a_m^T]^T$, its $l_{2,1}$-norm is $\sum_1^m \|a_i\|_2$, and a_i is a row of A.

B. Solving the Built MSBE Model

Due to the properties of the $l_{\frac{2}{3}}$-norm, (4) is a nonconvex and nondifferentiable problem, making it challenging to solve. Considering that HQS exhibits high efficiency and precision when handling such minimization problems [29], we derive an efficient method from HQS to solve (4).

Before presenting our method, we first recall the standard HQS method. Given a minimization problem

$$\min_u f(u) + g(Gu) \tag{5}$$

with quadratic $f(u)$, nonquadratic $g(Gu)$, and an operator G, HQS first converts problem (5) into

$$\min_{u,z} \left\{ J(u,z) = f(u) + g(z) + \frac{\rho}{2}\|Gu - z\|_2^2 \right\} \tag{6}$$

with an auxiliary variable z, and then decomposes problem (6) into alternating subproblems

$$\min_u f(u) + \frac{\rho}{2}\|Gu - \hat{z}\|_2^2 \tag{7}$$

and

$$\min_z g(z) + \frac{\rho}{2}\|G\hat{u} - z\|_2^2. \tag{8}$$

Finally, the generated subproblems are independently handled to obtain solutions to the original problem (5). According to REMARK 2 in [30], $\{\dots, J(u^k, z^k), J(u^k, z^{k+1}), J(u^{k+1}, z^{k+1}), \dots\}$ converges after sufficient iterations. Due to their good adaptability and performance, HQS and its variants have also been adopted in many other applications [29], [31], [32].

Since (4) is a half-quadratic problem, we apply the HQS strategy, yielding

$$L^{k+1} = \arg\min_L \|b^k \otimes L - D\|_2^2 + \gamma\|\nabla L - W^k\|_2^2, \tag{9}$$

$$b^{k+1} = \arg\min_b \|b \otimes L^{k+1} - D\|_2^2 + \mu\|b - V^k\|_2^2, \tag{10}$$

$$W^{k+1} = \arg\min_W \alpha\|W\|_{\frac{2}{3}} + \frac{\gamma}{2}\|\nabla L^{k+1} - W\|_2^2, \tag{11}$$

and

$$V^{k+1} = \arg\min_V \beta\|V\|_{2,1} + \frac{\mu}{2}\|V - b^{k+1}\|_2^2, \tag{12}$$

where the parameters γ and μ are greater than zero.

C. Solving Subproblems (9) to (12)

For the robustness of MSBE, some simple but efficient methods are employed by our framework to solve subproblems (9) to (12) independently and obtain closed-form solutions.

1) Obtaining Intermediate LIs: By FFTs [33], the solution of quadratic (9) is

$$L^{k+1}=F^{-1}\Big(\frac{\overline{F}(b^k)\circ F(D)+\gamma\overline{F}(\nabla)\circ F(W^k)}{\overline{F}(b^k)\circ F(b^k)+\gamma\overline{F}(\nabla)\circ F(\nabla)}\Big), \quad (13)$$

where $F(\cdot)$ is an FFT operation; $F^{-1}(\cdot)$ and $\overline{F}(\cdot)$ are its inversion and conjugate, respectively; and "$\circ$" is the dot product.

2) Estimating Final BKs: Because the intensity of LIs is not beneficial for robust blur estimation, we estimate BKs in a more favorable gradient domain. To eliminate adverse gradients, we first apply a smoothing algorithm [25] to the gradients of intermediate LIs and then use the refined gradients to estimate BKs. Therefore, problem (10) is reformulated as

$$b^{k+1}=\arg\min_{b}\frac{1}{2}\|b\otimes\nabla L_s^{k+1}-\nabla D\|_2^2+\frac{\mu}{2}\|b-V^k\|_2^2, \quad (14)$$

where ∇L_s^{k+1} is the refined ∇L^{k+1} generated by the algorithm of [25]. By FFTs, the solution of quadratic (14) is

$$b^{k+1}=F^{-1}\Big(\frac{\overline{F}(\nabla L_s^{k+1})\circ F(\nabla D)+\mu F(V^k)}{\overline{F}(\nabla L_s^{k+1})\circ F(\nabla L_s^{k+1})+\mu}\Big). \quad (15)$$

To prevent the estimation of BKs, especially large BKs, from converging to local optimal solutions, we estimate BKs using (15) in the multiscale process mentioned in Section 2.

3) Updating W and V: To efficiently obtain closed-form solutions, we apply the pointwise GST$_q$ algorithm [23] to problem (11), that is,

$$(W^{k+1})_i=GST_q\big((\nabla L_s^{k+1})_i,\frac{\alpha}{\gamma}\big), \quad (16)$$

where p=$\frac{2}{3}$ and $(W^{k+1})_i$ and $(\nabla L_s^{k+1})_i$ are the points of W^{k+1} and ∇L_s^{k+1}, respectively. The GST$_q$ is described in **Algorithm 1**.

Algorithm 1 GST$_q$

Input: $z=(\nabla L_s^{k+1})_i$, $\lambda=\frac{\alpha}{\gamma}$, $q=\frac{2}{3}$ and J
$\delta_q^{GST}(\lambda)\leftarrow\big(2\lambda(1-q)\big)^{\frac{1}{2-q}}$, $\theta_q^{GST}(\lambda)\leftarrow\lambda q\big(2\lambda(1-q)\big)^{\frac{q-1}{2-q}}$
$\beta_q^{GST}(\lambda)\leftarrow\delta_q^{GST}(\lambda)$+$\theta_q^{GST}(\lambda)$
If $|y|\le\beta_q^{GST}(\lambda)$
  $GST_q(y,\lambda)\leftarrow0$
Else Iterate from $j=0$ to J
  $j=0$ and $x^j=|y|$
  $x^{j+1}\leftarrow|y|-\lambda q(x^j)^{q-1}$
  $GST_q(y,\lambda)\leftarrow sgn(y)x^j$
EndIf
Output: $GST_q(y,\lambda)$

The objective function of subproblem (12) is

$$\frac{\beta}{\mu}\sum_{i=1}^{m}\|v_i\|_2+\frac{1}{2}\sum_{i=1}^{m}\|v_i-b_i^{k+1}\|_2^2, \quad (17)$$

where v_i and b_i^{k+1} are the i-th rows; thus, solving (12) yields

$$v_i^{k+1}=\arg\min_{v_i}\frac{\beta}{\mu}\sum_{i=1}^{m}\|v_i\|_2+\frac{1}{2}\sum_{i=1}^{m}\|v_i-b_i^{k+1}\|_2^2. \quad (18)$$

Obviously, problem (18) is soft-thresholding, so its closed-form solution [24] is

$$v_i^{k+1}=\begin{cases}\dfrac{\|b_i^{k+1}\|_2-\frac{\beta}{\mu}}{\|b_i^{k+1}\|_2}b_i^{k+1} & \|b_i^{k+1}\|_2>\dfrac{\beta}{\mu}\\ 0 & \|b_i^{k+1}\|_2\le\dfrac{\beta}{\mu}\end{cases},i=1,2,...,m. \quad (19)$$

D. Proposed MSBE framework

According to Subsection 3.3, we summarize the proposed MSBE scheme as **Algorithm 2** and **Algorithm 3**. In **Algorithm 3**, the number of layers in an image pyramid is determined by its kernel size, where i is the layer label of the image pyramid. Considering the nature of real BKs, we impose the constraints b≥0 and $\|b\|_1$=1 on b after each iteration. These constraints amount to setting the harmful components of the estimated b to zero and normalizing the estimated b.

Algorithm 2 Restoring Intermediate LIs

Input: D, b^k, and parameters α and β
Initialize: $L^0=D$ and $W^0=\nabla L^0$
For $k=0$ to K
  Compute L^{k+1} using (13)
  Update W^{k+1} using **Algorithm 1**
EndFor
Apply the l_0-smoothing algorithm [25] to ∇L^{k+1} to obtain ∇L_s^{k+1}
Output: ∇L_s^{k+1}

Algorithm 3 Robust Blur Estimation

Input: D and parameters β and (μ,μ_{max})
Initialize: coarsest $b^{0,1}=0$, $V^{0,1}=b^{0,1}$ and $V^{0,1}=b^{0,1}$
Repeat in a coarse-to-fine mode $(i=1,2,...,I)$
  While $\mu<\mu_{max}$ **Do**
    Compute $L_s^{k+1,i}$ using **Algorithm 2**
    Compute $b^{k+1,i}$ using (15)
    Update $V^{k+1,i}$ using (19)
    $\mu\leftarrow\mu\times2$
  EndWhile
  Upscale image $\nabla L_s^{k+1,i}$ to next finer layer
Until the estimation of the finest layer is finished
Output: b^{k+1} (Finest BKs)

IV. ID Phase

Once the MSBE is finished, we use the estimated BKs as the input of the ID phase. To generate high-quality ID results for non-low-light degraded images, we use the EPLL algorithm [34] to restore the final LIs. Given degraded images

TABLE I: Average SSDEs of the LIs Corresponding to the Degraded **im01** and Average RT (Levin Dataset)

Algorithms	Average SSDEs	Average RT
Pan	36.0057	2 min 59 sec
Yan	35.1840	3 min 33 sec
Jin	48.4888	1 min 55 sec
Bai	59.3848	60 sec
Chen	33.1646	2 min 3 sec
Proposed	**29.8616**	**43 sec**

TABLE II: Average SSDEs of the LIs Corresponding to the Degraded **im02** and Average RT (Levin Dataset)

Algorithms	Average SSDEs	Average RT
Pan	36.2418	2 min 57 sec
Yan	39.8594	3 min 27 sec
Jin	64.8607	2 min 7 sec
Bai	94.8294	58 sec
Chen	40.5545	2 min 2 sec
Proposed	**31.3482**	**42 sec**

TABLE III: Average SSDEs of the LIs Corresponding to the Degraded **im03** and Average RT (Levin Dataset)

Algorithms	Average SSDEs	Average RT
Pan	23.4432	2 min 56 sec
Yan	25.6223	3 min 24 sec
Jin	69.0822	2 min 9 sec
Bai	53.6291	58 sec
Chen	**22.7214**	1 min 50 sec
Proposed	22.8917	**41 sec**

and estimated BKs, the EPLL algorithm computes the final LIs by

$$\hat{o} = \big(\lambda_1 B^T B + \lambda_2 \sum_j Q_j^T Q_j\big)^{-1} \big(\lambda_2 B^T d + \lambda_2 \sum_j Q_j^T c_j\big), \tag{20}$$

where B is a BCCB convolutional matrix generated by b; $\hat{o}$ and d denote the final LIs and degraded images, respectively; matrix Q_j is used to select patches from $\hat{o}$; c_j is an auxiliary variable that satisfies $\hat{c}_j$=$Q_j\hat{o}$; and λ_1>0 and λ_2>0 are model parameters.

Although we use the EPLL algorithm to solve ID problems, other SotA restoration algorithms [35] are also applicable in this phase. For low-light degraded images, we turn to the SotA deconvolution approach of Whyte et al. [36] to obtain the final LIs.

V. Experimental Results

Comprehensive BID experiments are implemented on the publicly available Levin [22], Kohler [37], Sun [28] and Lai datasets [38]. The experimental results are assessed based on the SR, SSDE [22], PSNR, SSIM [39], vision effect and RT. Our BID algorithm competes with several SotA BID algorithms to evaluate its performance.

A. Experiments on Levin

As illustrated in Fig. 4, the synthetic Levin dataset has four clear images, eight uniform BKs, and 32 generated degraded

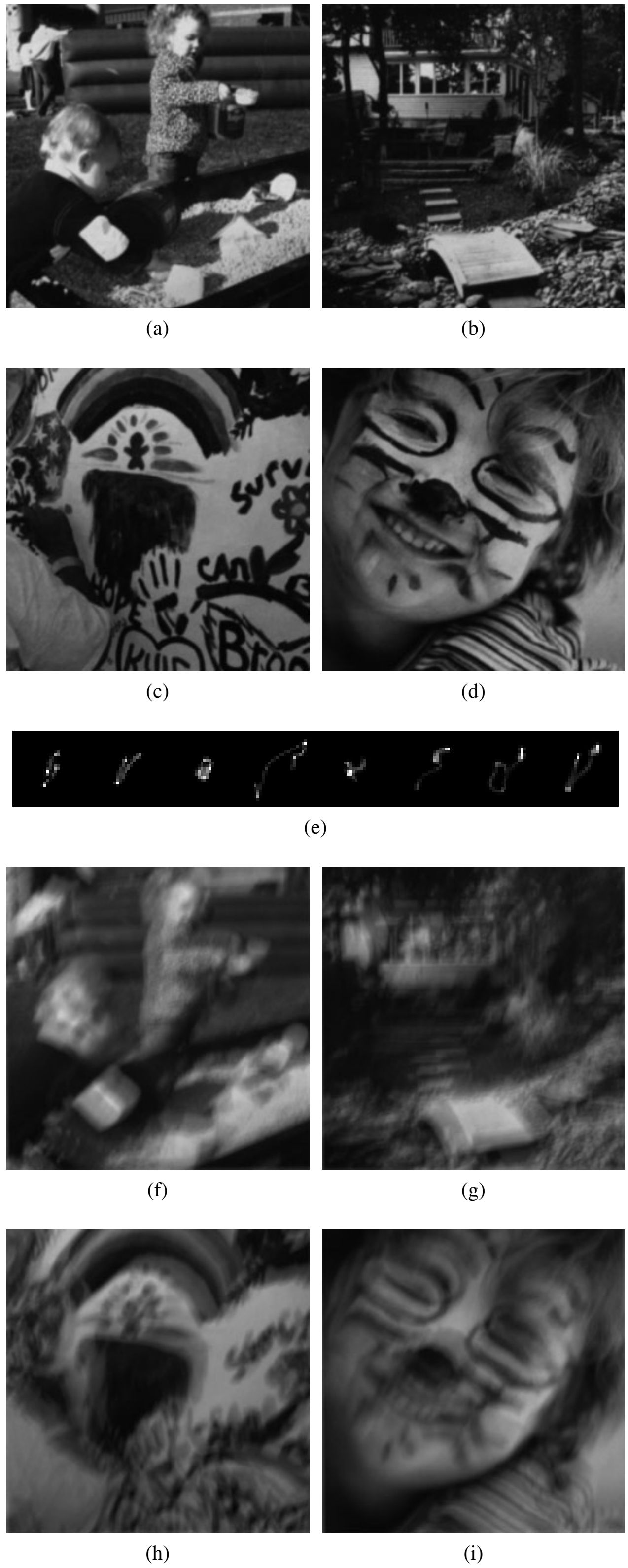

Fig. 4: Image Instances and BKs in Levin Dataset. (a)-(d) Clear images, (e) BKs (Kernel1 to Kernel8), and (f)-(i) degraded images.

images. The Levin dataset is an authoritative dataset with a long history and is used in many BID studies. In this dataset, the SR, SSDE, and vision effect are utilized to assess the generated results. To obtain SRs, the SSDEs of LIs are first divided by standard SSDEs, resulting in an error-ratio (ER) matrix, and the proportion of matrix components that are not

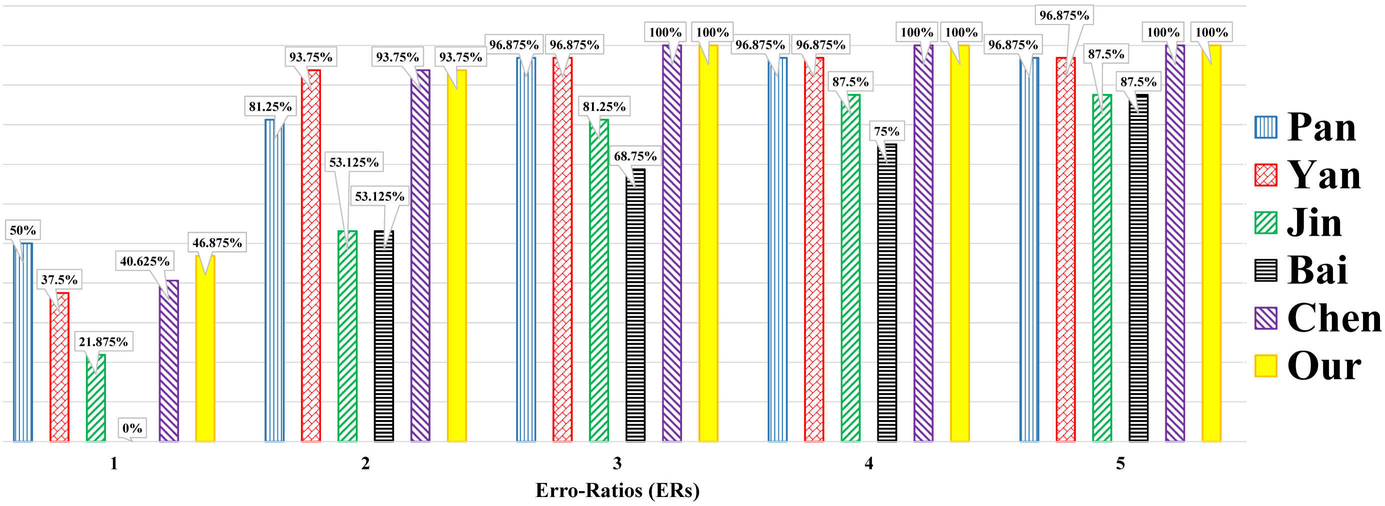

Fig. 5: SRs of the BID Algorithms

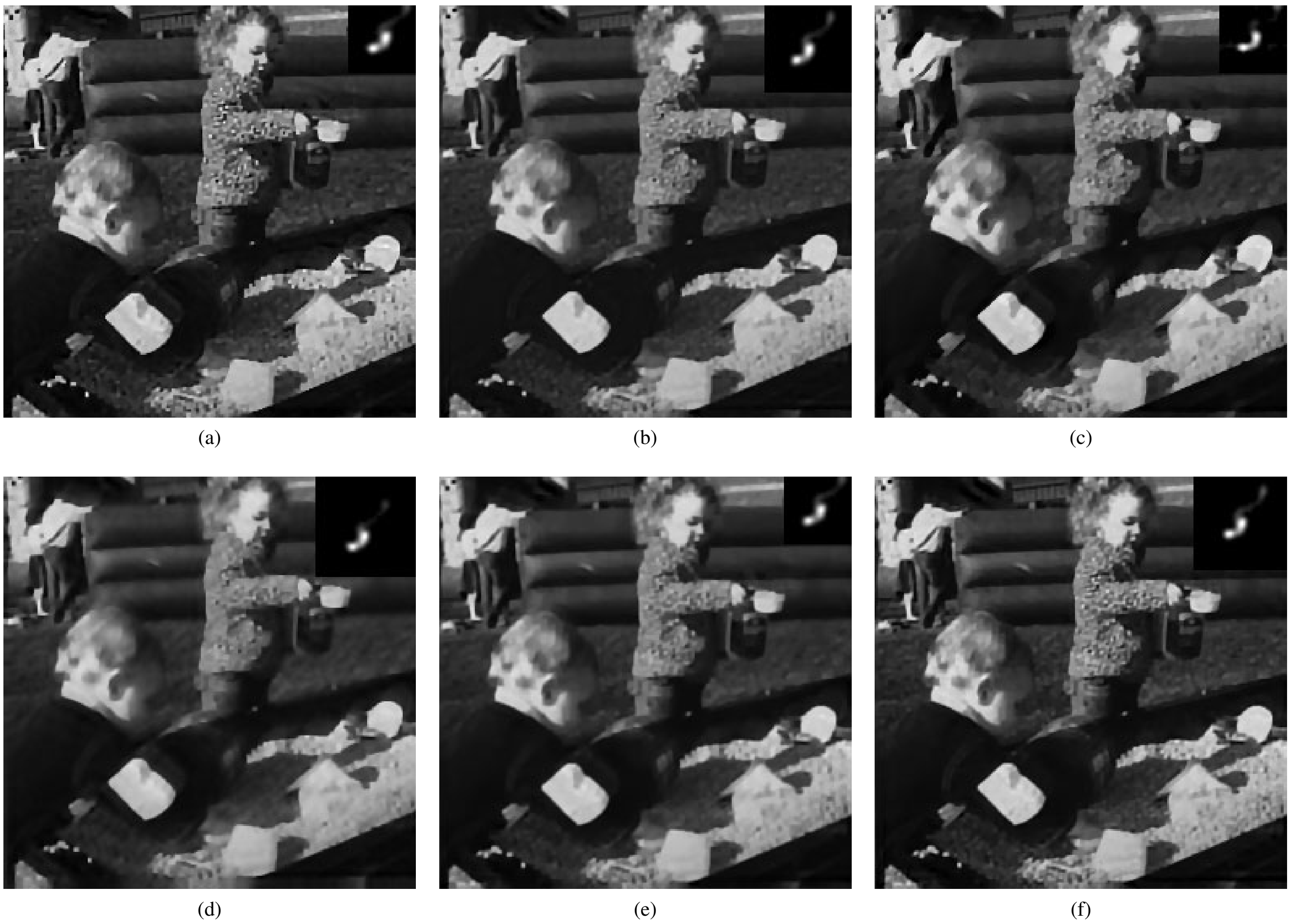

Fig. 6: LIs Corresponding to Degraded Image **im01_ker06** (Levin Dataset). (a) Pan, SSDE = 38.0779; (b) Yan, SSDE = 21.6973; (c) Jin, SSDE = 39.0838; (d) Bai, SSDE = 61.7870; (e) Chen, SSDE = 20.7844; and (f) Proposed, **SSDE = 17.6711**.

greater than a fixed ER is subsequently computed. Like in most BID algorithms, we adopt integers from 1 to 5 as fixed ERs. The BID algorithms evaluated in this experiment are the proposed, Pan [5], Yan [6], Jin [8], Bai [9], and Chen [11] algorithms. For precision and efficiency, the parameters of our BID algorithm are α=1.5e-3, β=5e-2, γ=1e-3, and (μ_0, μ_{max})=(5e-3, 1e10). The other BID algorithms adopt the recommended configurations and default settings.

The experimental results obtained after handling the Levin dataset are reported in TABLEs I to V and Figs. 5 and 6, where TABLEs I to V record the average SSDE values and average RT; Fig. 5 depicts the SRs of all BID algorithms; and Fig. 6 shows the vision effects of LIs.

In TABLEs I to V, the average SSDEs obtained by the proposed BID algorithm all rank highest except for the SSDE in TABLE III, which ranks second. Therefore, the proposed

TABLE IV: Average SSDEs of the LIs Corresponding to the Degraded **im04** and Average RT (Levin Dataset)

Algorithms	Average SSDEs	Average RT
Pan	100.6482	2 min 56 sec
Yan	118.8942	3 min 24 sec
Jin	164.2414	1 min 56 sec
Bai	117.1542	59 sec
Chen	43.5844	1 min 50 sec
Proposed	**32.2169**	**42 sec**

TABLE V: Average SSDEs of All LIs and Average RT (Levin Dataset)

Algorithms	Average SSDEs	Average RT
Pan	49.0847	2 min 57 sec
Yan	54.8900	3 min 27 sec
Jin	86.6683	2 min 2 sec
Bai	81.2494	59 sec
Chen	35.0062	1 min 56 sec
Proposed	**29.0796**	**42 sec**

TABLE VI: Average PSNRs (dB) and SSIMs of the LIs Corresponding to the Degraded **Church** and Average RT (Kohler Dataset)

Algorithms	Avg. PSNRs	Avg. SSIMs	Avg. RT
Pan	31.3052	0.8072	3 h 53 min 1 sec
Yan	31.3597	0.8106	2 h 47 min 21 sec
Jin	31.2399	0.8190	1 h 44 min 9 sec
Bai	30.8642	0.7444	31 min 51 sec
Chen	31.3320	0.8117	2 h 7 min 52 sec
Proposed	**31.5116**	**0.8415**	**7 min 46 sec**

BID algorithm has an overall advantage over the other BID algorithms in terms of SSDE.

As shown in Fig. 5, all the BID algorithms except for the proposed and Chen algorithms fail to achieve a 100% SR given an ER$\leq$5. Compared to the Chen algorithm, our BID algorithm achieves higher SRs in the cases of ER=1 and ER=2. Therefore, the proposed BID algorithm has higher SRs than do the other BID algorithms.

As illustrated in Fig. 6, the salient features of LIs are successfully reconstructed. Our BID algorithm obtains finer LIs with more details and fewer artifacts, while the LIs generated by the other BID algorithms are either smoother or have apparent artifacts.

As reported by TABLEs I to V, our BID algorithm needs the least average RT to handle the degraded images in the Levin dataset, which is 29% less than that of the second-ranked algorithm. The RT advantages of our BID algorithm and the results in the tables and figures demonstrate that it obtains better BID results at faster speeds when handling the Levin dataset.

B. Experiments on Kohler

The synthetic Kohler dataset has four clear images, 12 nonuniform BKs, and 48 generated degraded images, as shown in Fig. 7. The PSNR, SSIM, and vision effect are employed to assess the results obtained on the Kohler dataset. Each degraded image corresponds to 199 clear images, so each of the generated LIs can obtain 199 PSNRs and 199 SSIMs. We adopted the average PSNRs and SSIMs as the final scores. The BID algorithms considered in this experiment are the proposed, Pan, Yan, Jin, Bai, and Chen algorithms. To balance precision and efficiency, the parameters of our BID algorithm are α=4.5e-3, β=0.5, γ=1.5e-2, and (μ_0, μ_{max})=(8e-3, 1e10). The other BID algorithms adopt the recommended configurations and default settings.

The experimental results obtained after the Kohler dataset was processed are reported in TABLEs VI to X and Fig. 8,

(a) (b) (c) (d) (e) (f) (g) (h)

Fig. 7: Image Instances in Kohler Dataset. (a)-(d) Clear images, and (e)-(h) degraded images

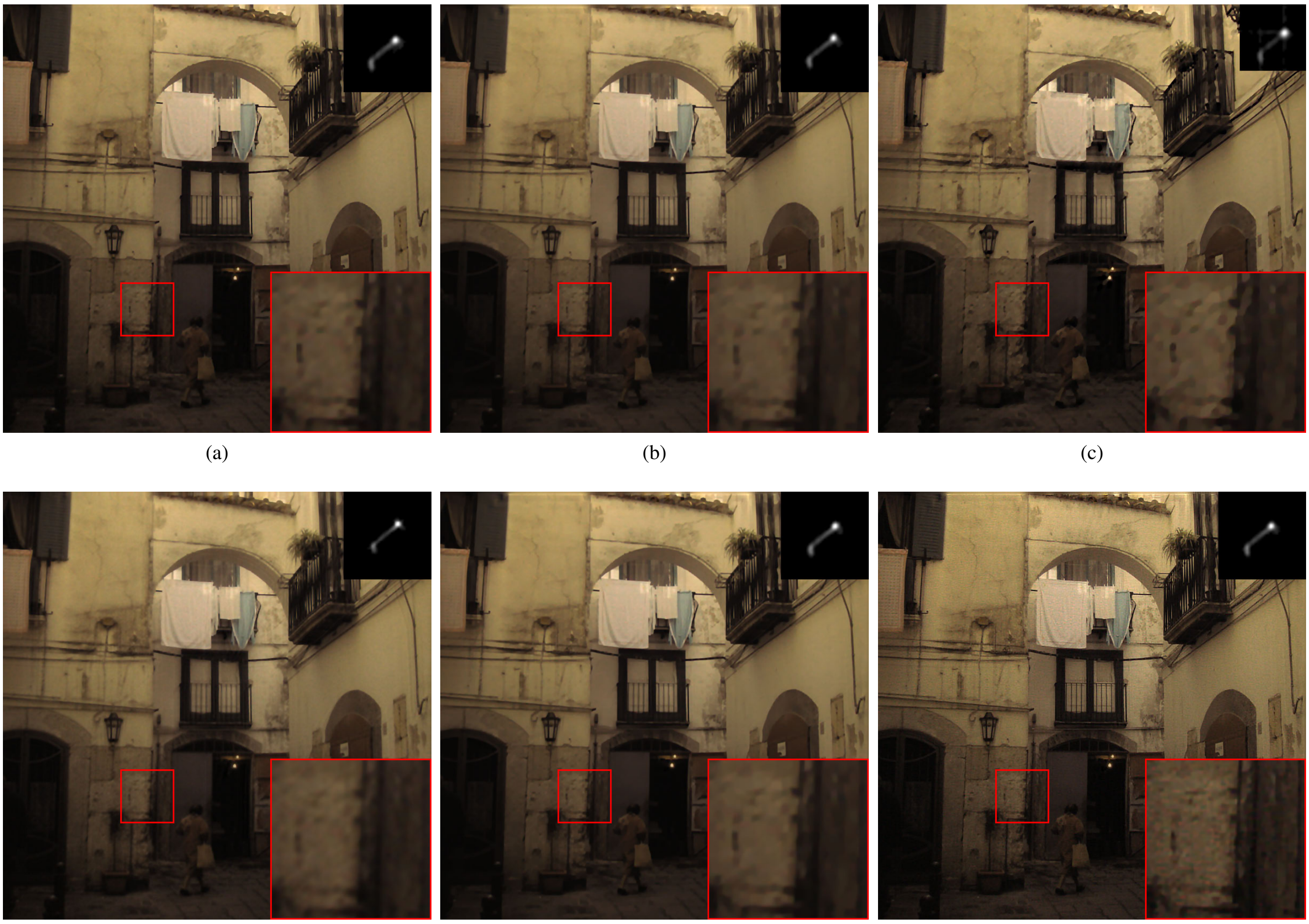

(a) (b) (c)

(d) (e) (f)

Fig. 8: LIs Corresponding to the Degraded Image **Blurry3_1** (Kohler Dataset). (a) Pan, P = 33.0534 dB, S = 0.8474; (b) Yan, P = 32.9545 dB, S = 0.8488; (c) Jin, P = 32.5276 dB, S = 0.8342; (d) Bai, P = 32.8319 dB, S = 0.8528; (e) Chen, P = 32.9809 dB, S = 0.8474; and (f) Proposed, **P = 33.3032 dB**, **S = 0.8759**. The letters P and S stand for PSNR and SSIM, respectively.

TABLE VII: Average PSNRs (dB) and SSIMs of the LIs Corresponding to the Degraded **Clock** and Average RT (Kohler Dataset)

Algorithms	Avg. PSNRs	Avg. SSIMs	Avg. RT
Pan	30.7652	0.6494	3 h 51 min 42 sec
Yan	**30.7931**	0.6522	3 h 1 min 53 sec
Jin	30.4372	0.6729	1 h 48 min 20 sec
Bai	30.4303	0.6194	31 min 20 sec
Chen	30.7698	0.6420	2 h 20 min 31 sec
Proposed	30.7824	**0.6919**	**8 min 2 sec**

TABLE VIII: Average PSNRs (dB) and SSIMs of the LIs Corresponding to the Degraded **Backyard** and Average RT (Kohler Dataset)

Algorithms	Avg. PSNRs	Avg. SSIMs	Avg. RT
Pan	31.9411	0.8395	3 h 52 min 17 sec
Yan	31.9036	0.8435	3 h 1 min 13 sec
Jin	31.5405	0.8350	1 h 42 min 30 sec
Bai	31.6772	0.8271	31 min 41 sec
Chen	31.8755	0.8416	2 h 4 min
Proposed	**32.0918**	**0.8674**	**7 min 55 sec**

TABLE IX: Average PSNRs (dB) and SSIMs of the LIs Corresponding to the Degraded **Roof** and Average RT (Kohler Dataset)

Algorithms	Avg. PSNRs	Avg. SSIMs	Avg. RT
Pan	30.4078	0.7235	3 h 58 min 43 sec
Yan	30.3675	0.7153	3 h 3 min 34 sec
Jin	30.3843	0.7412	1 h 49 min 1 sec
Bai	30.2264	0.7112	33 min 4 sec
Chen	30.3809	0.7163	2 h 4 min 30 sec
Proposed	**30.6210**	**0.7615**	**7 min 52 sec**

TABLE X: Average PSNR Scores (dB) and Average SSIM Scores of All LIs and Average RT of BID Algorithms (Kohler Dataset)

Algorithms	Avg. PSNRs	Avg. SSIMs	Avg. RT
Pan	31.1048	0.7549	3 h 53 min 56 sec
Yan	31.1060	0.7554	2 h 58 min 30 sec
Jin	30.9005	0.7670	1 h 46 min
Bai	30.7995	0.7255	31 min 59 sec
Chen	31.0895	0.7529	2 h 9 min 13 sec
Proposed	**31.2517**	**0.7906**	**7 min 54 sec**

(a)

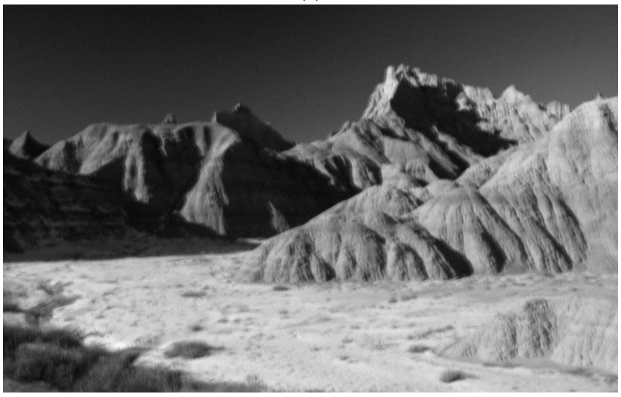

(b)

Fig. 9: Image Instances in Sun Dataset. (a) A clear image, and (b) a degraded image corresponding to (a).

where TABLEs VI to X record the average PSNRs and SSIMs of the generated LIs and the average RT of the BID algorithms; and Fig. 8 shows the vision effects of the generated LIs.

For TABLEs VI to X, the average PSNRs and SSIMs obtained by our BID algorithm all rank highest except for the average PSNR in TABLE VII, which ranks second by 0.0107 dB. Therefore, the proposed BID algorithm has overall advantages over the other BID algorithms regarding the PSNR and SSIM.

As illustrated in Fig. 8, the prominent features of the generated LIs are successfully reconstructed. The LIs obtained by the proposed BID algorithm look clearer with more features, while the LIs generated by the other BID algorithms are either smoother or have apparent artifacts.

As shown in TABLEs VI to X, the proposed BID algorithm requires the least average RT to handle the degraded images in the Kohler dataset, whereas the RT required by the other BID algorithms varies from 4 to 30 times that of our BID algorithm. The significant RT advantages of our BID algorithm when combined with the data from TABLEs VI to X and Fig. 8 demonstrate that it obtains better BID results at faster speeds on the Kohler dataset than do the other BID algorithms.

C. Experiments on Sun

The synthetic Sun dataset has 80 clear images, 8 uniform BKs from the Levin Dataset, and 640 generated degraded images, as shown in Fig. 9. The PSNR and SSIM are used to comprehensively assess the quality of the generated LIs and the precision of the estimated BKs. The BID algorithms considered in this experiment are the proposed, Pan, Yan, Jin, Bai, and Chen algorithms. For precision and efficiency, the parameters of our BID algorithm are α=4.5e-3, β=0.4, γ=1.2e-3, and (μ_0, μ_{max})=(1e-3, 1e10). The other BID algorithms adopt the recommended configurations and default settings.

The experimental results obtained after the Sun dataset was

TABLE XI: Average PSNRs (dB) and SSIMs of All LIs (Sun Dataset)

Algorithms	Average PSNRs	Average SSIMs
Pan	33.2080	0.6695
Yan	33.2118	0.6816
Jin	32.3686	0.5948
Bai	32.7381	0.6601
Chen	33.2414	0.6850
Proposed	**33.3414**	**0.6919**

TABLE XII: Average PSNRs (dB) and SSIMs of All Estimated Blur Kernels (Sun Dataset)

Algorithms	Average PSNRs	Average SSIMs
Pan	38.8058	0.5316
Yan	39.0148	0.5309
Jin	35.5939	0.4308
Bai	35.5212	0.5376
Chen	39.1981	0.5338
Proposed	**39.8330**	**0.6060**

TABLE XIII: Average PSNRs (dB) of the Estimated Kernel1 to Kernel4 (Sun Dataset)

Algorithms	Kernel1	Kernel2	Kernel3	Kernel4
Pan	43.9324	47.8211	36.3888	37.3750
Yan	43.5245	48.3420	36.2877	37.3282
Jin	38.7068	37.3822	34.5098	36.3750
Bai	38.4519	37.4016	35.2302	36.2824
Chen	43.5461	49.4996	36.5919	37.6840
Proposed	**44.2457**	**49.5937**	**37.2826**	**38.1886**

TABLE XIV: Average PSNRs (dB) of the Estimated Kernel5 to Kernel8 (Sun Dataset)

Algorithms	Kernel5	Kernel6	Kernel7	Kernel8
Pan	36.5921	36.0360	34.9935	37.3079
Yan	37.7309	36.0906	35.4331	37.3817
Jin	32.8804	35.5425	34.6377	34.7166
Bai	32.7377	35.1907	34.4177	34.4578
Chen	36.7071	36.2483	35.4797	37.8282
Proposed	**37.9909**	**36.9401**	**36.3353**	**38.0870**

TABLE XV: Average SSIMs of the Estimated Kernel1 to Kernel4 (Sun Dataset)

Algorithms	Kernel1	Kernel2	Kernel3	Kernel4
Pan	0.5912	0.5695	0.4750	0.5012
Yan	0.6135	0.5718	0.4216	0.4928
Jin	0.5744	0.4022	0.3573	0.4774
Bai	0.6128	0.5011	0.5309	0.5780
Chen	0.5920	0.5715	0.4810	0.4901
Proposed	**0.6379**	**0.5931**	**0.5368**	**0.6098**

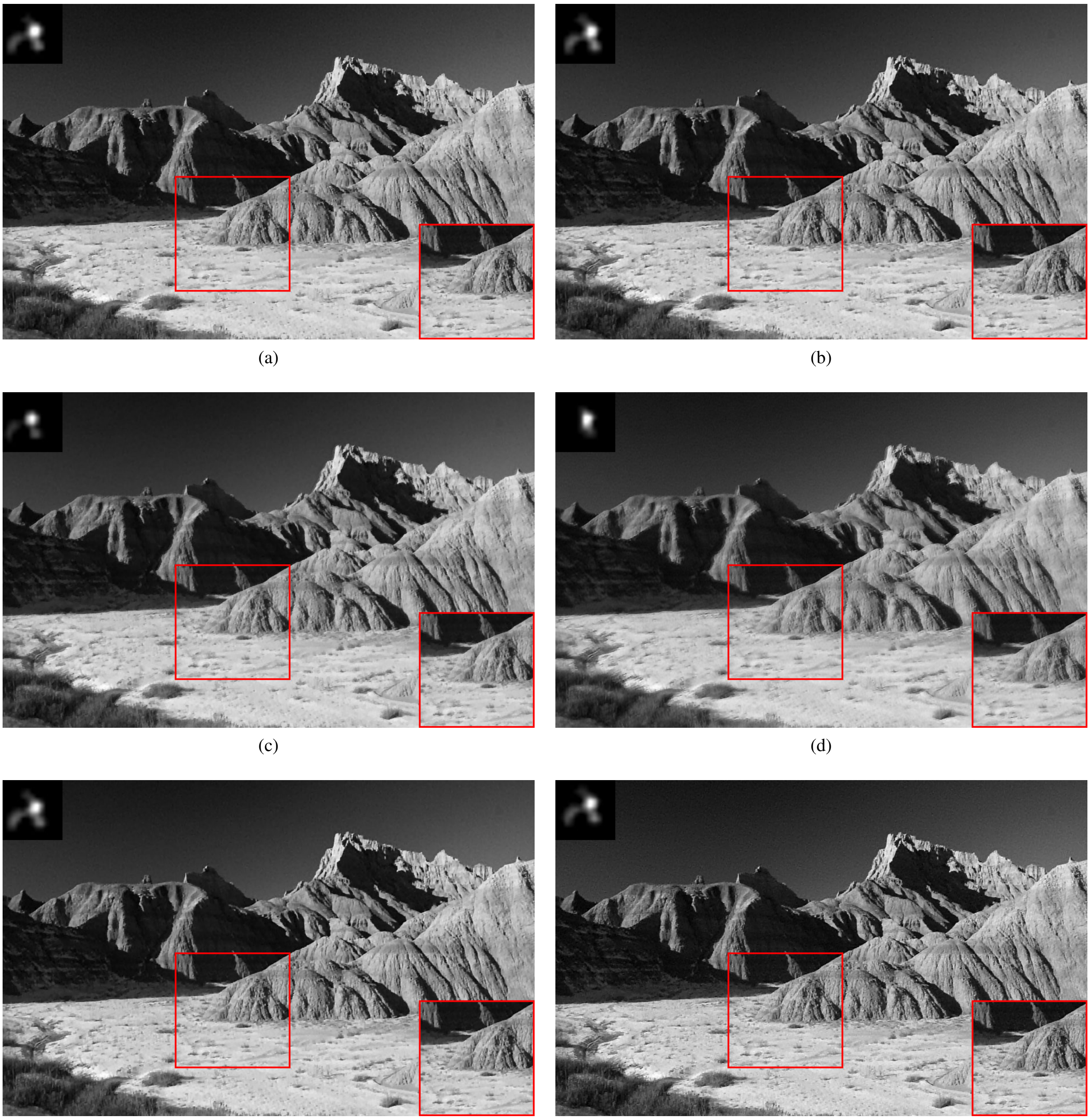

(a) (b) (c) (d) (e) (f)

Fig. 10: LIs Corresponding to Degraded Image **3_5_blurred** (Sun Dataset). (a) Pan, P = 32.7885 dB, S = 0.7395; (b) Yan, P = 33.1063 dB, S = 0.7968; (c) Jin, P = 32.4652 dB, S = 0.6781; (d) Bai, P = 32.5621 dB, S = 0.7158; (e) Chen, P = 32.8095 dB, S = 0.7616; and (f) Proposed, **P = 34.5013 dB**, **S = 0.8774**. The letters P and S stand for PSNR and SSIM, respectively.

TABLE XVI: Average SSIMs of the Estimated Kernel5 to Kernel8 (Sun Dataset)

Algorithms	Kernel5	Kernel6	Kernel7	Kernel8
Pan	0.6795	0.4803	0.3917	0.5641
Yan	0.7068	0.4813	0.4090	0.5506
Jin	0.3686	0.4259	0.4014	0.4391
Bai	0.4476	0.5093	0.5068	0.6143
Chen	0.6717	0.4972	0.4049	0.5620
Proposed	**0.7218**	**0.5787**	**0.5144**	**0.6554**

processed are reported in TABLEs XI to XVI and Fig. 10, where TABLEs XI records the average PSNRs and SSIMs of the generated LIs; TABLEs XII to XVI records the average PSNRs and SSIMs of the estimated BKs; and Fig. 10 shows the vision effects of the generated LIs.

Regarding the generated LIs, the proposed BID algorithm has advantages over the other BID algorithms because the average PSNRs and SSIMs obtained by our BID algorithm are both the highest. Regarding the estimation precision of BKs, the data in TABLE XII also demonstrate the advantages of the proposed BID algorithm over other BID algorithms. TABLEs XI to XVI show that the precise estimation of the BKs is beneficial for obtaining high-quality LIs and that our approach for kernel estimation is very effective.

As illustrated in Fig. 10, the salient features of the gener-

(a)

(b)

Fig. 11: Image Instances in the Synthetic Lai Dataset.(a) A clear image, and (b) a degraded image corresponding to (a).

TABLE XVII: Average PSNRs of Generated LIs (Manmade, Natural, and People in Synthetic Lai Dataset)

Algorithms	Manmade	Natural	People
Pan	30.1062 dB	31.8391 dB	33.6048 dB
Yan	30.0514 dB	31.6473 dB	33.9924 dB
Jin	29.7702 dB	31.9955 dB	34.4580 dB
Bai	29.6952 dB	31.7172 dB	34.0229 dB
Chen	29.7536 dB	31.9730 dB	34.1742 dB
Proposed	**31.8167 dB**	**33.6403 dB**	**35.5937 dB**

TABLE XVIII: Average PSNRs of Generated LIs (Saturated, Text, and All in Synthetic Lai Dataset)

Algorithms	Saturated	Text	All
Pan	33.7426 dB	34.0532 dB	32.6692 dB
Yan	33.5965 dB	32.1979 dB	32.2971 dB
Jin	33.5262 dB	31.2059 dB	32.1912 dB
Bai	33.7680 dB	31.3832 dB	32.1173 dB
Chen	33.5779 dB	33.0309 dB	32.5019 dB
Proposed	**34.9755 dB**	**34.1239 dB**	**34.0300 dB**

ated LIs are successfully reconstructed. The LIs obtained by the proposed BID algorithm look more natural and sharper than those generated by the other BID algorithms.

D. Experiments on Synthetic Lai

As shown in Fig. 11, the Lai dataset also includes synthetic data consisting of 25 clear images, four nonuniform BKs and

TABLE XIX: Average SSIMs of the Generated LIs (Manmade, Natural, and People in Synthetic Lai Dataset)

Algorithms	Manmade	Natural	People
Pan	0.5760	0.7911	0.8334
Yan	0.5840	0.7721	0.8431
Jin	0.5707	0.7838	0.8241
Bai	0.5964	0.8016	0.8340
Chen	0.5424	0.8008	0.8530
Proposed	**0.6371**	**0.8706**	**0.9006**

TABLE XX: Average SSIMs of the Generated LIs (Saturated, Text, and All in Synthetic Lai Dataset)

Algorithms	Saturated	Text	All
Pan	0.6733	0.7211	0.7190
Yan	0.6701	0.6775	0.7094
Jin	0.6555	0.6663	0.7001
Bai	0.6891	0.6959	0.7234
Chen	0.6633	0.7347	0.7189
Proposed	**0.7389**	**0.7458**	**0.7786**

TABLE XXI: Average RT of Processing Real-World Degraded Images

Algorithms	Average RT
Pan	1 h 27 min 31 sec
Yan	4 h 33 min 57 sec
Jin	11 h 50 min 31 sec
Bai	54 min 33 sec
Chen	1 h 3 min 2 sec
Proposed	**4 min 59 sec**

100 degraded images. The degraded images in the dataset are classified into Manmade images, Natural images, People images, Saturated images, and Text images. Considering the speeds of some BID algorithms in this experiment, we select 5 degraded images from each category for testing. We use the proposed, Pan, Yan, Jin, Bai, and Chen algorithms to process these degraded images and assess the experimental results using the PSNR, SSIM, and vision effect. For precision and efficiency, the parameters of our BID algorithm are α=6e-3, β=0.3, γ=2e-4, and (μ_0, μ_{max})=(5e-4, 1e10). The other BID algorithms adopt the recommended configurations and default settings.

The results are reported in Fig. 12 and TABLEs XVII to XX, where Fig. 12 demonstrates the vision effects of the generated LIs, and TABLEs XVII to XX record the PSNR scores and SSIM scores of the generated LIs. With regard to the definition of the generated LIs, the proposed BID algorithm has advantages over the other BID algorithms because the average PSNRs and average SSIMs obtained by the proposed BID algorithm are both the highest. As illustrated in Fig. 12, the salient features of the generated LIs are successfully reconstructed. The LIs obtained by the proposed BID algorithm look more natural and sharper than those generated by the other BID algorithms.

E. Experiments on the Real-World Dataset

The experimental data are also from the famous Lai dataset and include degraded images of different sizes, contents, and

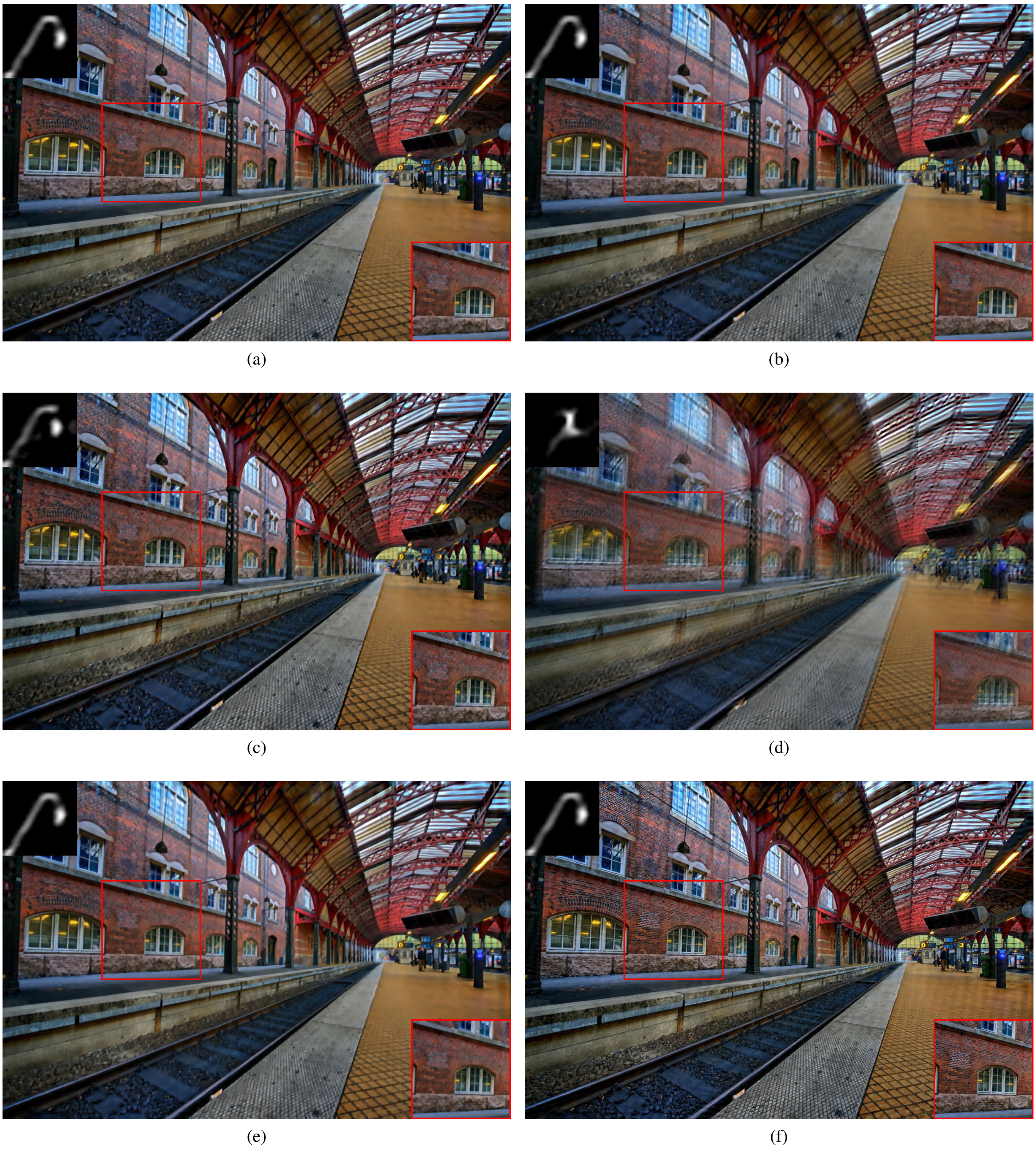

Fig. 12: LIs Corresponding to Degraded Image **Manmade_02_kernel_01**. (a) Pan, (b) Yan, (c) Jin, (d) Bai, (e) Chen, and (f) Proposed.

blur types. Due to the absence of clear images and true BKs, the vision effect is used to assess the restored results of the BID algorithms. The BID algorithms evaluated in this experiment are the proposed, Pan, Yan, Jin, Bai, and Chen algorithms. For ideal vision effects, the parameters of our BID algorithm are α=8e-4, β=5e-2, γ=1.5e-3, and (μ_0, μ_{max})=(3.5e-3, 1e10). The other BID algorithms adopt recommended configurations and default settings.

The experimental results obtained after handling the real-world degraded images are reported in Figs. 13 to 16 and TABLE XXI, where Figs. 13 to 16 demonstrate the vision effects of the generated LIs and TABLE XXI records the average RT. The results in the figures cover all types of images commonly found in daily life and scientific research, thus truly and fully demonstrating the performances of the BID algorithms.

Regarding the vision effect, as shown in Figs. 13 to 16, the prominent features of the LIs are successfully reconstructed. Our BID algorithm obtains finer LIs with more details and fewer artifacts, while the LIs generated by other BID algorithms are either overly smooth or have apparent artifacts.

As reported in TABLE XXI, the proposed BID algorithm requires the least average RT to handle real-world degraded images in the Lai dataset, whereas the RT required by the other BID algorithms varies from 11 to 143 times that of our BID algorithm. The significant RT advantages of our BID algorithm and the results in TABLE XXI and Figs. 13 to 16 demonstrate that it obtains better BID results at faster speeds

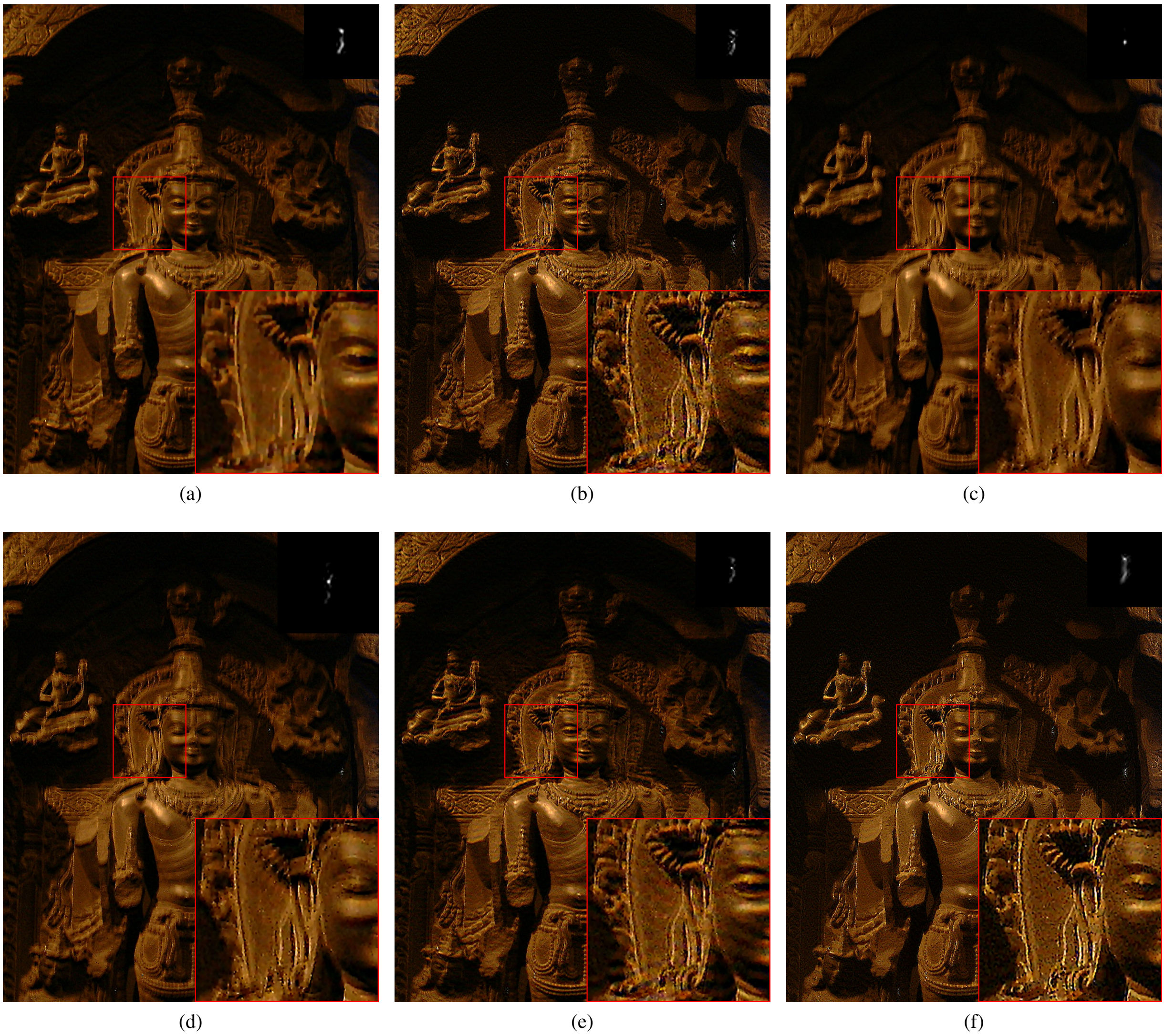

Fig. 13: LIs Corresponding to Degraded **Lyndsey**. (a) Pan, (b) Yan, (c) Jin, (d) Bai, (e) Chen, and (f) Proposed.

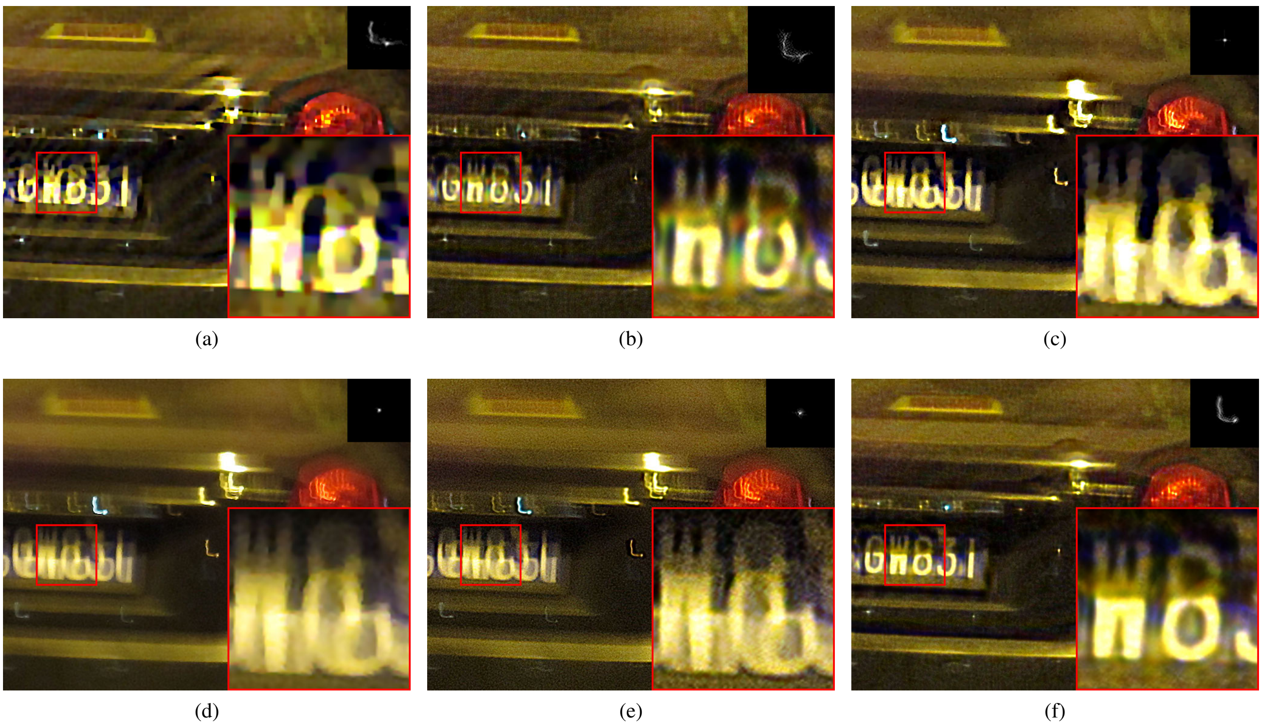

Fig. 14: LIs Corresponding to Degraded **Car**. (a) Pan, (b) Yan, (c) Jin, (d) Bai, (e) Chen, and (f) Proposed.

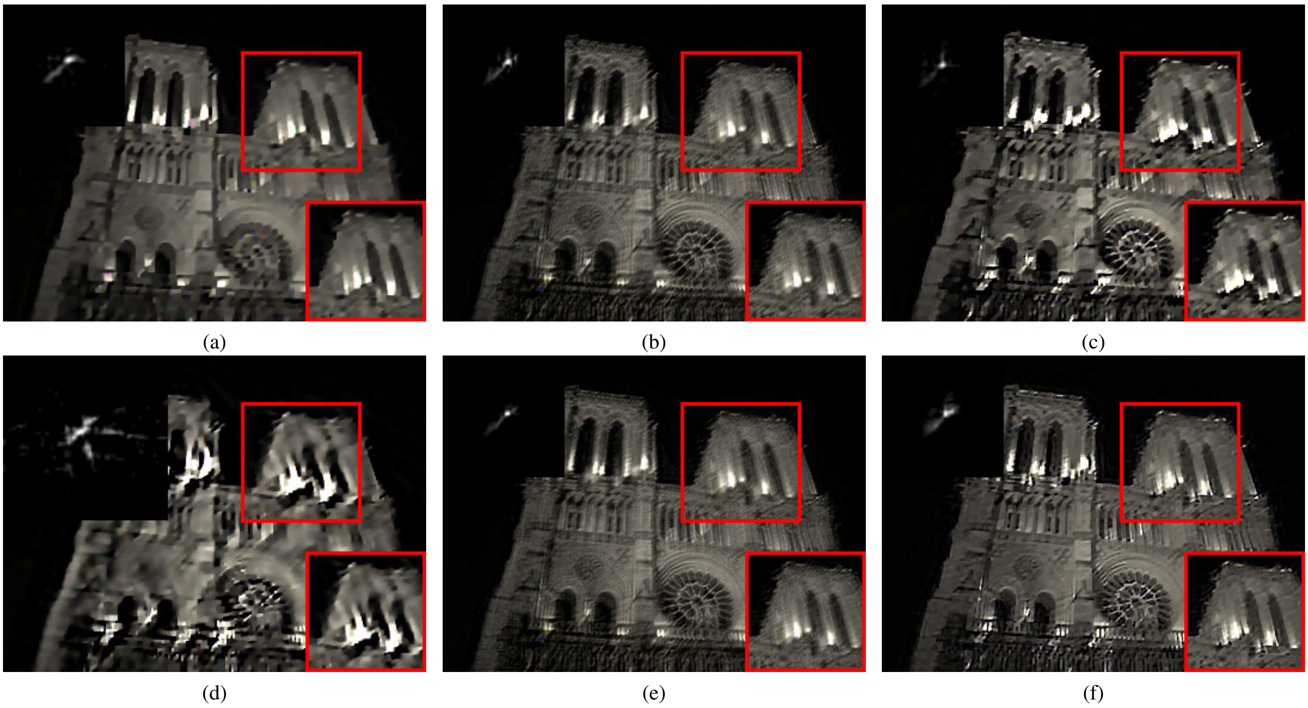

Fig. 15: LIs Corresponding to Degraded **Building**. (a) Pan, (b) Yan, (c) Jin, (d) Bai, (e) Chen, and (f) Proposed.

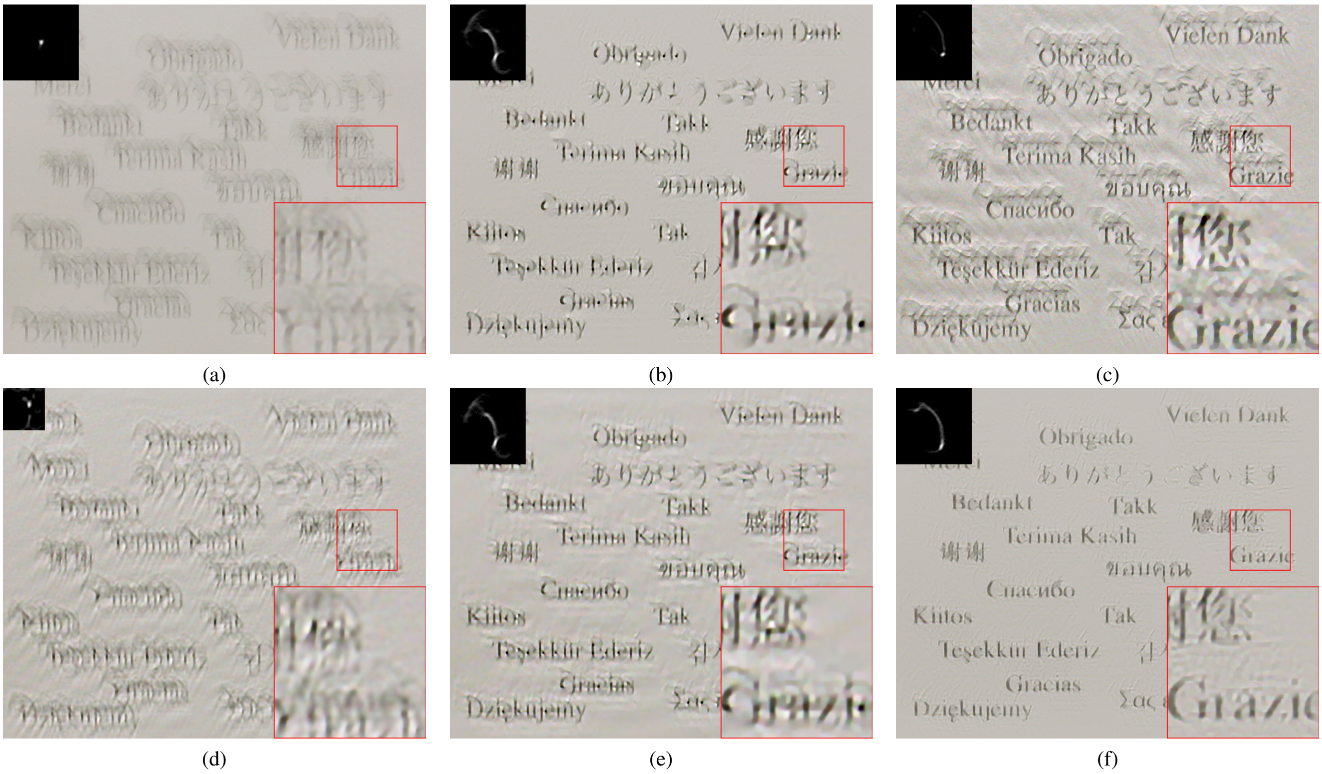

Fig. 16: LIs Corresponding to Degraded **Text**. (a) Pan, (b) Yan, (c) Jin, (d) Bai, (e) Chen, and (f) Proposed.

than do the other BID algorithms when handling real-world degraded images.

F. Convergence and Performance

In this subsection, the performances of the BID algorithms and the convergence of our BID algorithm are analyzed.

TABLE XXII lists the objective results of the BID algorithm in above experiments, where the first data represents PNSR score, the second data represents SSIM score, and the third data represents SSDE score. The data in TABLE XXII indicate that our BID algorithm performs better than the other BID algorithms on mainstream datasets under various objective criteria. The other BID algorithms exhibit significant fluctuations in their performance when processing different datasets, which also reveals that our BID algorithm has more stable performance and better adaptability.

The RT performance is also an important consideration for practical applications. The Pan, Yan, Jin, Bai, and Chen

TABLE XXII: Quantitative Results of All BID Algorithms

Algorithms	Levin Dataset	Kohler Dataset	Sun Dataset	Synthetic Lai Dataset
Pan	— / — / 49.0847	31.1048 dB / 0.7549 / —	33.2080 dB / 0.6695 / —	32.6692 dB / 0.7190 / —
Yan	— / — / 54.8900	31.1060 dB / 0.7554 / —	33.2118 dB / 0.6816 / —	32.2971 dB / 0.7094 / —
Jin	— / — / 86.6683	30.9005 dB / 0.7670 / —	32.3686 dB / 0.5948 / —	32.1912 dB / 0.7001 / —
Bai	— / — / 81.2494	30.7995 dB / 0.7255 / —	32.7381 dB / 0.6601 / —	32.1173 dB / 0.7234 / —
Chen	— / — / 35.0062	31.0895 dB / 0.7529 / —	33.2414 dB / 0.6850 / —	32.5019 dB / 0.7189 / —
Proposed	— / — / **29.0796**	**31.2517 dB / 0.7906** / —	**33.3414 dB / 0.6919** / —	**34.0300 dB / 0.7786** / —

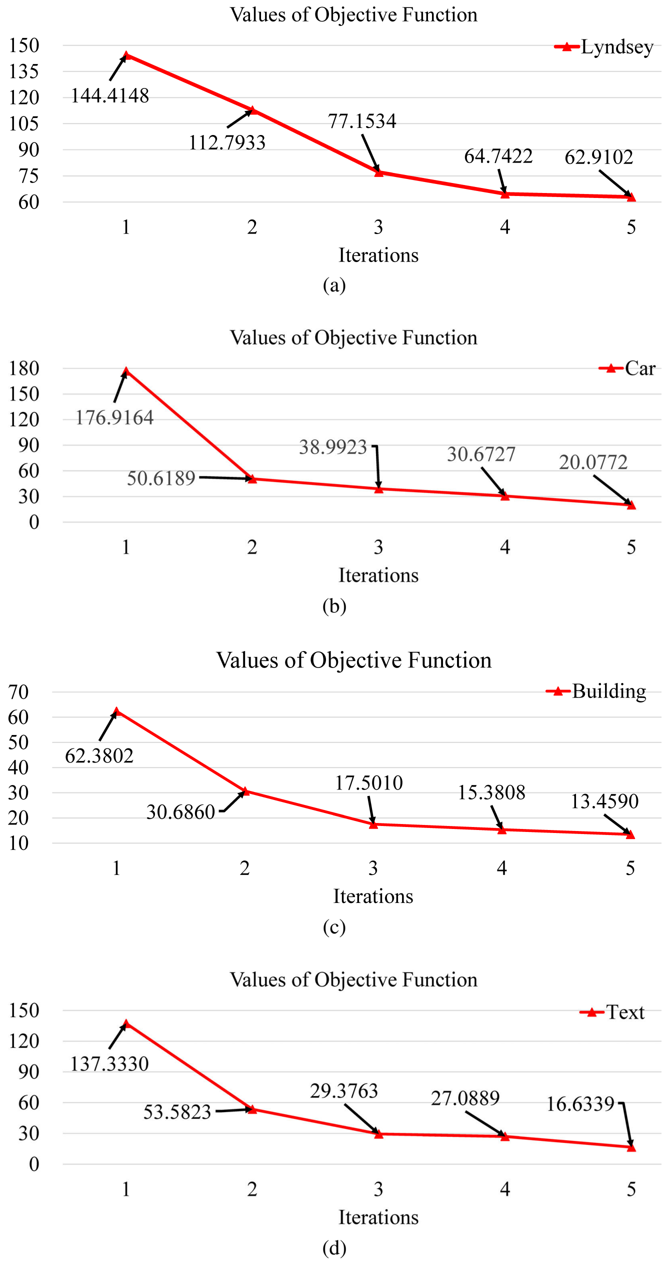

Fig. 17: Value Changes of (4). (a) Lyndsey, (b) Car, (c) Building, and (d) Text.

algorithms spend much time computing the weights, EC, scaled l_p-norm, RGTV, and LMG, respectively, whereas the proposed BID algorithm avoids costly computations. Therefore, the our BID algorithm will be more favorable than the other BID algorithms in applications.

We have observed the fast convergence of our BID algorithm in previous experiments. We also demonstrate its convergence through the value changes of (4) shown in Fig. 17. The changes in the figure occur when iteratively estimating the final BKs. The trends show that the values of (4) decrease continuously during the iteration; that is, our BID algorithm converges.

VI. Conclusions

In this study, a novel BID model is established using an HLG prior and sparse $l_{2,1}$-regularization and is solved by a method derived from the HSQ. The generated subproblems are independently solved by FFTs, GST$_q$, and iterative soft-thresholding to obtain precise BKs. To obtain high-quality LIs, the EPLL algorithm and the algorithm of Whyte et al. are employed. We conduct comprehensive BID experiments on multiple datasets, including the Levin, Kohler, Sun, and Lai datasets, and compare the experimental results obtained by the participating BID algorithms. The results show the comprehensive advantages of our BID algorithm regarding the SR, SSDE, PSNR, SSIM, vision effect, and RT. In the future, we will extend our research to other related fields.

References

[1] Rob Fergus, Barun Singh, Aaron Hertzmann, Sam T. Roweis, and William T. Freeman, “Removing Camera Shake from a Single Photograph,” *ACM Transactions on Graphics*, vol. 25, no. 3, pp 787-794, 2006

[2] Jiangxin Dong, Jinshan Pan, Zhixun Su, and Ming-Hsuan Yang, “Blind Image Deblurring with Outlier Handling,” *Proceedings of the IEEE International Conference on Computer Vision*, 22-29 October, 2017, Venice, Italy, pp 2478-2486

[3] Taiebeh Askari Javaran, Hamid Hassanpour, and Vahid Abolghasemi, “Local Motion Deblurring Using an Effective Image Prior Based on Both the First- and Second-Order Gradients,” *Machine Vision & Applications*, vol. 28, no. 3-4, pp 431-444, 2017

[4] Y. Liu, W. Dong, D. Gong, L. Zhang and Q. Shi, “Deblurring Natural Image Using Super-Gaussian Fields,” *Lecture Notes in Computer Science: Proceedings of the European Conference on Computer Vision*, 8-14 September, 2018, Munich, Germany, pp 452-468

[5] Jinshan Pan, Zhouchen Lin, Zhixun Su, and Ming-Hsuan Yang, “Robust Kernel Estimation with Outliers Handling for Image Deblurring,” *Proceedings of the IEEE Conference on Computer Vision and Pattern Recognition*, 26 June - 1 July, 2016, Las Vegas, USA, pp 2800-2808

[6] Yanyang Yan, Wenqi Ren, Yuanfang Guo, Rui Wang, and Xiaochun Cao, “Image Deblurring via Extreme Channels Prior,” *Proceedings of the IEEE Conference on Computer Vision and Pattern Recognition*, 21-26 July, 2017, Honolulu, USA, pp 4003-4011

[7] Fengjun Zhang, Wei Lu, Hongmei Liu, and Fei Xue, “Natural Image Deblurring Based on L0-Regularization and Kernel Shape Optimization,” *Multimedia Tools & Applications*, vol. 77, no. 20, pp 26239-26257, 2018

[8] Meiguang Jin, Stefan Roth, and Paolo Favaro , “Normalized Blind Deconvolution,” *Lecture Notes in Computer Science: Proceedings of the European Conference on Computer Vision*, 8-14 September, 2018, Munich, Germany, pp 668-684

[9] Yuanchao Bai, Gene Cheung, Xianming Liu, and Wen Gao, “Graph-Based Blind Image Deblurring from a Single Photograph,” *IEEE Transactions on Image Processing*, vol. 28, no. 3, pp 1404-1418, 2019

[10] Liuge Yang, and Hui Ji, “A variational EM framework with adaptive edge selection for blind motion deblurring,” *Proceedings of the IEEE/CVF Conference on Computer Vision and Pattern Recognition*, 16-20 June, 2019, Long Beach, USA, pp 10167-10176

[11] Liang Chen, Faming Fang, Tingting Wang, and Guixu Zhang, “Blind Image Deblurring with Local Maximum Gradient Prior,” *Proceedings of the IEEE/CVF Conference on Computer Vision and Pattern Recognition*, 16-20 June, 2019, Long Beach, USA, pp 1742-1750

[12] Saeed Anwar, Cong Phuoc Huynh, and Fatih Porikli, “Image Deblurring with a Class-Specific Prior,” *IEEE Transactions on Pattern Analysis and Machine Intelligence*, vo. 41, no. 9, pp 2112-2130, 2019

[13] Jun Liu, Ming Yan, and Tieyong Zeng, “Surface-Aware Blind Image Deblurring,” *IEEE Transactions on Pattern Analysis and Machine Intelligenc*, vol. 43, no. 3, pp 1041-1055, 2021

[14] Bin Sheng, Ping Li, Xiaoxin Fang, Ping Tan, and Enhua Wu, “Depth-Aware Motion Deblurring Using Loopy Belief Propagation,” *IEEE Transactions on Circuits and Systems for Video Technology*, vol. 30, no. 4, pp 955-969, 2020

[15] Liyuan Pan, Richard Hartley, Miaomiao Liu, and Yuchao Dai, “Phase-Only Image Based Kernel Estimation for Single Image Blind Deblurring,” *Proceedings of the IEEE/CVF Conference on Computer Vision and Pattern Recognition*, 16-20 June, 2019, Long Beach, USA, pp 6034-6043

[16] Juncai Peng, Yuanjie Shao, and Changxin Gao, “Joint Image Deblurring and Matching with Feature-Based Sparse Representation Prior,” *Pattern Recognition*, vol. 103, pp 107300, 2020

[17] Xianfeng Ding, Tingting Wei, Yiyuan Wang, and Jiaxin Li, “Low Rank Tensor Completion via Schatten-2/3 Norm and Schatten-1/2 Norm,” *IAENG International Journal of Applied Mathematics*, vol. 53, no. 1, pp 317-328, 2023

[18] Xiaofeng Zhu, Jiangzhang Gan, Guangquan Lu, Jiaye Li, and Shichao Zhang, “Spectral Clustering via Half-Quadratic Optimization,” *World Wide Web*, vol. 23, no. 3, pp 1969-1988, 2020

[19] Zhijun Luo, Zhibin Zhu, and Benxin Zhang, “An SCADTV Nonconvex Regularization Approach for Magnetic Resonance Imaging,” *IAENG International Journal of Computer Science*, vol. 48, no. 4, pp 1013-1020, 2021

[20] Christian J. Schuler, Michael Hirsch, Stefan Harmeling, and Bernhard Scholkopf, “Learning to Deblur,” *IEEE Transactions on Pattern Analysis and Machine Intelligence*, vol. 38, no. 7, pp 1439-1451, 2016

[21] Kaihao Zhang, Wenhan Luo, Yiran Zhong, Lin Ma, Bjorn Stenger, Wei Liu, and Hongdong Li, “Deblurring by Realistic Blurring,” *Proceedings of the IEEE/CVF Conference on Computer Vision and Pattern Recognition*, 13-19 June, 2020, Virtual, pp 2737-2746

[22] Anat Levin, Yair Weiss, Fredo Durand, and William T. Freeman, “Understanding Blind Deconvolution Algorithms,” *IEEE Transactions on Pattern Analysis and Machine Intelligence*, vol. 33, no. 12, pp 2354-2367, 2011

[23] Wangmeng Zuo, Deyu Meng, Lei Zhang, Xiangchu Feng, and David Zhang, “A Generalized Iterated Shrinkage Algorithm For Non-Convex Sparse Coding,” *Proceedings of the IEEE International Conference on Computer Vision*, 2-8 December, 2013, Sydney, Australia, pp 217-224

[24] Haoyang Liu, and Rina F. Barber, “Between Hard and Soft Thresholding: Optimal Iterative Thresholding Algorithms,” *Information and Inference: A Journal of the IMA*, vol. 9, no. 4, pp 899-933, 2020

[25] i Xu, Cewu Lu, Yi Xu, and Jiaya Jia, “Image Smoothing via L0 Gradient Minimization,” *ACM Transactions on Graphics*, vol. 30, no. 6, pp 1-12, 2011

[26] Yair Weiss, and William T. Freeman, “What Makes a Good Model of Natural Images?” *Proceedings of the IEEE Conference on Computer Vision and Pattern Recognition*, 17-22 June, 2007, Minneapolis, USA, pp 1-8

[27] Mingzhu Shi, Tingting Han, and Shuaiqi Liu, “Total Variation Image Restoration Using Hyper-Laplacian Prior with Overlapping Group Sparsity,” *Signal Processing*, vol. 126, pp 65-76, 2016

[28] Libin Sun, Sunghyun Cho, Jue Wang, and James Hays, “Edge-Based Blur Kernel Estimation Using Patch Priors,” *Proceedings of the IEEE International Conference on Computational Photography*, 19-21 April, 2013, Cambridge, USA, pp 1-8

[29] Zhi-Feng Pang, Hui-Li Zhang, Shousheng Luo, and Tieyong Zeng, “Image Denoising Based on the Adaptive Weighted TV^p Regularization,” *Signal Processing*, vol. 167, pp 107325, 2020

[30] Mila Nikolova, and Michael K. Ng, “Analysis of Half-Quadratic Minimization Methods for Signal and Image Recovery,” *SIAM Journal on Scientific Computing*, vol. 27, no. 3, pp 937-966, 2005

[31] Congcong Xu, Bo Yang, Fupei Guo, Wenfeng Zheng, and Philippe Poignet, “Sparse-View CBCT Reconstruction via Weighted Schatten p-Norm Minimization,” *Optics Express*, vol. 28, no. 24, pp 35469-35482, 2020

[32] Siyuan Peng, Wee Ser, Badong Chen, and Zhiping Lin, “Robust Semi-Supervised Nonnegative Matrix Factorization for Image Clustering,” *Pattern Recognition*, vol. 111, pp 107683, 2021

[33] K. R. Rao, D. N. Kim and J. Hwang, *Fast Fourier Transform-Algorithms and Applications*. Dordrecht: Springer, 2011.

[34] Daniel Zoran, and Yair Weiss, “From Learning Models of Natural Image Patches to Whole Image Restoration,” *Proceedings of the IEEE International Conference on Computer Vision*, 6-13 November, 2011, Barcelona, Spain, pp 479-486

[35] Jingjing Cui, Guohua Peng, Quan Lu, and Zhengge Huang, “A Class of Nonstationary Upper and Lower Triangular Splitting Iteration Methods for Ill-Posed Inverse Problems,” *IAENG International Journal of Computer Science*, vol. 47, no. 1, pp 118-129, 2020

[36] Oliver Whyte, Josef Sivic, and Andrew Zisserman, “Deblurring Shaken and Partially Saturated Images,” *International Journal of Computer Vision*, vol. 110, no. 2, pp 185-201, 2014

[37] Rolf Kohler, Michael Hirsch, Betty Mohler, Bernhard Schölkopf, and Stefan Harmeling , “Recording and Playback of Camera Shake: Benchmarking Blind Deconvolution with a Real-World Database,” *Lecture Notes in Computer Science: Proceedings of the European Conference on Computer Vision*, 7-13 October, 2012, Florence, Italy, pp 27-40

[38] Wei-Sheng Lai, Jia-Bin Huang, Zhe Hu, Narendra Ahuja, and Ming-Hsuan Yang, “A Comparative Study for Single Image Blind Deblurring,” *Proceedings of the IEEE Conference on Computer Vision and Pattern Recognition*, 26 June - 1 July, 2016, Las Vegas, USA, pp 1701-1709

[39] De Rosal Igantius Moses Setiadi, “PSNR vs SSIM: Imperceptibility Quality Assessment for Image Steganography,” *Multimedia Tools & Applications*, vol. 80, no. 6, pp 8423–8444, 2021